Construction and Building Materials 328 (2022) 127116

Contents lists available at ScienceDirect

Construction and Building Materials

journal homepage: www.elsevier.com/locate/conbuildmat

Textile Reinforced Mortars (TRM) tensile behavior after high temperature exposure

Luis Estevan, Francisco B. Varona, F. Javier Baeza *, Benjamín Torres, David Bru

Department of Civil Engineering, University of Alicante, P.O. Box 99, 03080 Alicante, Spain

ARTICLE INFO

Keywords:
TRM
FRCM
High-temperature
Tensile strength
Non-destructive testing

ABSTRACT

Although one of the main advantages of Textile Reinforced Mortars (TRM) is their non-combustible character, their behavior against fire or high temperatures has not been sufficiently studied at present. This work analyzes the behavior of different commercial systems containing inorganic mortars and fabric reinforcements based on glass, carbon and basalt fibers, subjected to different temperature levels. To characterize the mechanical response of the different systems, non-destructive tests have been carried out to determine the dynamic modulus of elasticity of the different materials, and subsequent destructive tests to determine their strength and stress-strain relationship. For this purpose, the TRM coupons have been subjected to uniaxial tensile tests and the deformations have been monitored using LVDT (Linear Variable Displacement Transducer) sensors and DIC (Digital Image Correlation), in order to evaluate cracking patterns and failure modes. The results show, in general terms, that the mechanical capacity of these materials is seriously compromised at temperatures in the order of 400 to 600 °C, which can easily be reached during a fire inside a building. Therefore, it can be concluded that although these systems are erroneously perceived as fire resistant in many cases, they may require additional protection depending on the specific use for which they are intended.

1. Introduction

The application of composite materials in the field of structural repair and retrofitting has focused the attention of the scientific community during the last decades. Fiber Reinforced Polymers (FRP) have been successfully used in a wide range of projects and have been the target of a great deal of research [1]. However, these systems present some drawbacks, including the following: (i) the cost of the materials is relatively high compared to other reinforcement solutions; (ii) their application can pose challenges in the presence of moisture; (iii) the reduced permeability to water vapor may have deleterious effects in the frequent case of walls or columns affected by soil-induced-dampness, for example; (iv) in many cases there are incompatibilities with the base substrate, e.g., in the case of stone or masonry walls with rough finishes; (v) the application of these products is generally irreversible, which can be a serious disadvantage in interventions on buildings of historical or architectural value; (vi) the great sensitivity of epoxy resins to temperature means that the fire resistance of these materials is very low. These disadvantages can, in part, be solved by replacing the organic matrices with inorganic matrices, usually in the form of mortars. In this way, Textile Reinforced Mortars (TRM), also known in the scientific literature as Fabric Reinforced Cementitious Matrix (FRCM), have been developed in recent years [2,3]. These systems basically consist of the incorporation of one or more layers of fabrics in the form of meshes of glass, carbon, basalt, aramid or steel fibers (among other materials) inside a cementitious matrix, although other types might be used, such as hydraulic lime mortars.

The application of TRMs has been successfully used in recent years for the reinforcement of all types of structural elements. In case of stone or masonry structures, its effectiveness has been demonstrated for the reinforcement of walls [4,5], the confinement of columns [6,7] or the intervention in arches or vaults [8,9], among other purposes. Regarding concrete structures, their capacity has been analyzed mainly for the flexural reinforcement of beams or slabs [10,11], shear reinforcement [12] or columns confinement [13,14]. These and many other studies have led to the development of design guidelines for the practical application of this type of reinforcement, which, at present, are basically limited to the North American ACI 549.4R-20 [15] and the Italian CNR-DT 215/2018 [16].

Despite the advantages offered by TRMs, it is important to note that

* Corresponding author.
E-mail address: fj.baeza@ua.es (F.J. Baeza).

https://doi.org/10.1016/j.conbuildmat.2022.127116
Received 23 December 2021; Received in revised form 21 February 2022; Accepted 9 March 2022
Available online 14 March 2022

the adhesion between the fibers and the inorganic matrices is not as effective as in the case of FRP epoxy resins. The mortars cannot penetrate between the fibers and fully impregnate them, as the particle size is too large to occupy the space between the filaments. The consequence of this effect is that stress transfer between the matrix and the fibers is not uniform, resulting in what is commonly known as "telescopic failure", i.e., relative slip without perceptible damage: the outer fibers, where bond stress is greatest, break and the inner fibers, which remain relatively free, slip. This behavior can be improved, in part, by pre-impregnating the meshes with epoxy resin or other products before embedding them in the mortar matrix [17,18].

For the mechanical characterization of TRMs, rectangular coupons are typically used and tested in uniaxial tension according to the indications of the AC-434 guide [19] and the recommendations of RILEM TC 232-TDT [20]. During the last years, many interesting Round Robin tests have been carried out with extensive experimental campaigns and the involvement of different European laboratories: Carozzi et al. [21] studied different types of carbon fiber textiles and lime or cement-based matrices enriched with a low content of polymers; Leone et al. [22] proposed a similar investigation, using glass fiber fabrics and different types of mortars; in the case of Lignola et al. [23] they worked with basalt fiber fabrics. Other relevant works with different fabrics and matrices are, among others, those published by Caggegi et al. [24], D'Antino and Papanicolaou [25], Li et al. [26] and Hojdys and Krajewski [27]. Regarding the control of deformations in tests, in most experimental campaigns traditional measurement techniques are used, usually by means of LVDTs. However, it has been found in some works that monitoring through Digital Image Correlation (DIC) can increase the accuracy of the results and provide complementary information of great interest related to cracking patterns or failure modes [28,29].

To summarize all these studies, it can be assumed that the tensile behavior of TRMs essentially follows three distinct phases: (i) in the first phase of the test the mortar matrix remains uncracked and the slope of the stress-strain curve corresponds to the gross modulus of elasticity of the TRM, which could be estimated considering the equivalent homogenized section (matrix + fibers); (ii) the cracking of the matrix marks the beginning of the second phase, during which new cracks develop, whose number and spacing essentially depend on the properties of the fabric and its ability to adhere to the mortar; in this second phase the strains exhibit a significant increase, with very limited impact on the tensile stress, so that the modulus of elasticity is significantly reduced (in fact, this second branch of the stress-strain diagram is often idealized as a horizontal line, hence with a modulus equal to zero); and (iii) once the cracking of the matrix is fully developed, the stresses are transferred entirely to the textile material, resulting in an approximately linear final branch, whose slope is characterized by the stiffness of the fibers used. It is important to note, however, that in many cases and depending on the materials used, these three phases cannot be clearly distinguished from one another [30]. In terms of failure modes, three different types are usually observed: (a) fibers rupture in the central zone of the specimen; (b) fibers rupture in the vicinity of the anchorage zones; and (c) fibers slippage with respect to the mortar matrix, usually near the anchorage zones. The response of the TRM and the types of failure are usually associated with the anchorage system of the specimens to the test press, so some reports that specifically analyze this effect are therefore of interest [31].

In terms of the behavior of TRMs exposed to elevated temperatures, it seems clear that these materials offer better performance than FRPs, whose organic resins are extremely sensitive to heat and require specific protection against fire. The inherent non-combustible nature of inorganic mortars would imply that, a priori, they might be used without additional protection [32]. Nevertheless, little is currently known about the behavior of these materials exposed to high temperatures or under fire conditions, given the fact that relevant experimental results are scarce [33]. Regarding the tensile behavior of TRMs exposed to high temperatures -which is the main objective of this research- one of the first published works is that of Colombo et al. [34], who studied specimens with glass fiber meshes subjected to temperature levels of 200, 400 and 600 °C, and were able to prove that the material retains its properties at 200 °C, suffers a serious deterioration at 400 °C and loses all its mechanical capacity at 600 °C. De Andrade et al. [35] worked with carbon fibers (dry and pre-impregnated with polymers in aqueous suspension) and temperatures up to 600 °C. In the case of dry fibers, the first signs of deterioration were observed at 400 °C, obtaining a significant degradation at 600 °C. However, in the case of pre-impregnated fibers, although significant improvements were obtained up to 150 °C, the material suffered a significant loss for higher temperatures and was seriously damaged at 400 °C. This was attributed to the decomposition of the polymer by the effect of heat. In the works of Rambo et al. [36,37], basalt fiber meshes and temperature levels up to 1000 °C were used, obtaining similar results to the previous ones, with significant drops in strength over 400 °C and the material practically unusable at 600 °C. On the other hand, these studies provided an interesting analysis of the evolution of the cracking pattern of the specimens with increasing temperature by means of DIC. Donnini et al. [38] used carbon fiber meshes, dry and pre-impregnated with epoxy resin and quartz sand, although in this case the maximum exposure temperature was only 120 °C. Nonetheless, this temperature was sufficient to significantly degrade the material if the test was performed with hot specimens (in the case of pre-impregnated specimens), whilst other specimens kept their capacity if allowed to cool down and be tested at room temperature. In the case of Messori et al. [39], they worked with fiberglass meshes pre-impregnated with epoxy resin and temperatures up to 250 °C and found that the loss of mechanical properties of the material was not as severe as in other reported studies. The investigations by Nguyen et al. [40], Tlaiji et al. [41] and Homoro et al. [42] are also interesting. In these works, a press equipped with an oven was used, so that the uniaxial tensile test of TRMs was performed at the desired temperature. It should be noted that the size of the specimens was small, given the dimensions of the oven used. In all cases, glass fiber fabrics and temperature levels up to 600 °C were tested. Finally, in a recently published study by Dinh et al. [43], carbon fiber meshes were used, with a mortar matrix reinforced with metallic fibers. The exposure temperatures were up to 400 °C. It is interesting to see how the inclusion of fibers in the matrix was beneficial and increased the mechanical capacity of the TRM, even in those series subjected to maximum temperatures, thus being able to control the cracking of the mortar.

After analyzing the most recent publications on the behavior of TRM systems previously damaged by exposure to elevated temperatures, a lack of experimental studies and research in this field has been detected. In this context, the aim of this work is to analyze the degradation of the mechanical behavior of TRM systems after exposure to elevated temperatures. For this purpose, an extensive experimental campaign of both non-destructive and destructive tests has been carried out on different commercial systems with glass, carbon and basalt fiber meshes, different inorganic mortars and exposure temperatures up to 600 °C. This value of the maximum exposure temperature has been chosen because it has been shown that the mechanical capacity of these materials is severely compromised at this temperature range.

The present article has been structured in the following sections: Section 2 presents the materials studied and the description of the experimental campaign carried out; Section 3 shows the results obtained and their discussion, in terms of the degradation produced by the high temperatures on (i) the dynamic modulus of elasticity of the materials, (ii) the flexural and compressive strengths of the mortars, (iii) the stress-strain relationship of the different TRM systems, and (iv) the failure modes and crack distribution on the TRM specimens. Section 3 also includes a comparison of the results obtained in this investigation with the results of several relevant studies carried out by other authors. Finally, Section 4 highlights the main novel aspects contributed by the present study and shows the main conclusions obtained.

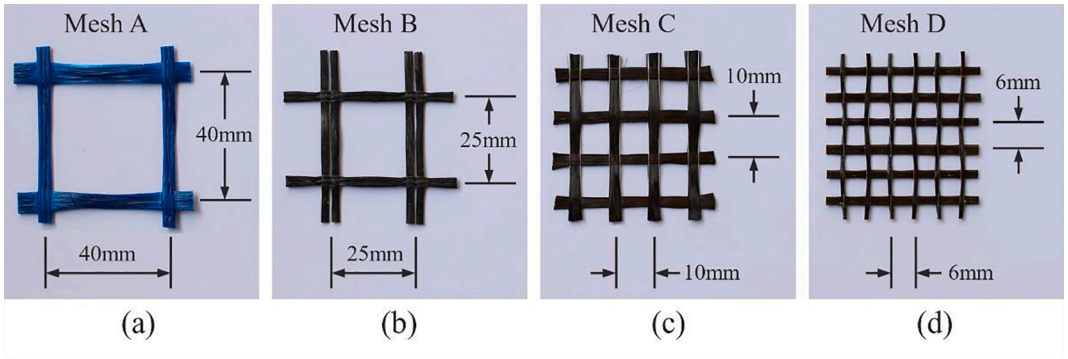

Fig. 1. Detail of the four meshes used: (a) Mapenet EM40 (glass); (b) Mapegrid G220 (glass); (c) Mapegrid C170 (carbon); (d) Mapegrid B250 (basalt).

Table 1
Properties of the meshes (values provided by the manufacturer).

	Mesh A	Mesh B	Mesh C	Mesh D
Product reference	Mapenet EM40	Mapegrid G220	Mapegrid C170	Mapegrid B250
Type of fiber	Glass	Glass	Carbon	Basalt
Mesh size (mm)	40 × 40	25 × 25	10 × 10	6 × 6
Weight (g/m^2)	270	225	170	250
Load-resistant area (mm^2/m)	35.82	35.27	48	38.91
Tensile strength (kN/m)	56.25	45	240	60
Tensile strength (MPa) [a]	1570	1276	5000	1542
Modulus of elasticity (GPa)	33	72	252	89
Elongation at failure (%)	4	1.8	2	1.8

[a] Values not supplied, obtained from tensile strength (kN/m) and load-resistant area.

2. Materials and methods

2.1. Textiles, mortars and TRM specimens

Four different types of fabrics have been used in this study, all of them provided by Mapei. Two of them are polymer-coated alkali resistant (AR) glass fiber meshes (Mapenet EM40 and Mapegrid G220). Another one is a high-strength carbon fiber mesh (Mapegrid C170). Finally, the fourth one is a primed-AR basalt fiber mesh (Mapegrid B250). In the following sections, these materials are referred to as A, B, C and D, respectively. Fig. 1 shows a detail of the different meshes used and Table 1 summarizes their main characteristics and mechanical properties, according to the manufacturer's specifications. In the particular case of Mapegrid C170 mesh, it should be noted that the tensile strength reported by the supplier seems to be too high for a carbon textile. Analyzing other studies with similar meshes, it has been found that the ultimate stress obtained experimentally is about 40% lower than the value provided for the individual filament [31,38]. The difference is basically due to the unavoidable unevenness in the stress distribution among the fiber bundles in the tests on fabric strips.

Regarding the mortars, two different types have been used, also supplied by Mapei: (i) MapeWall Render & Strengthen (for mesh type A), which is a ready-mixed mortar made from natural hydraulic lime, reactive inorganic compounds, natural sand, special admixtures and micro-fibers; and (ii) Planitop HDM Restauro (for meshes types B, C and D), which is a two-component fiber-reinforced mortar composed by hydraulic lime, Eco-Pozzolan, natural sand, special additives and synthetic polymers in water dispersion. Both mortars are hereinafter referred to as M1 and M2, respectively. In terms of their mechanical properties, the manufacturer declares a minimum compressive strength

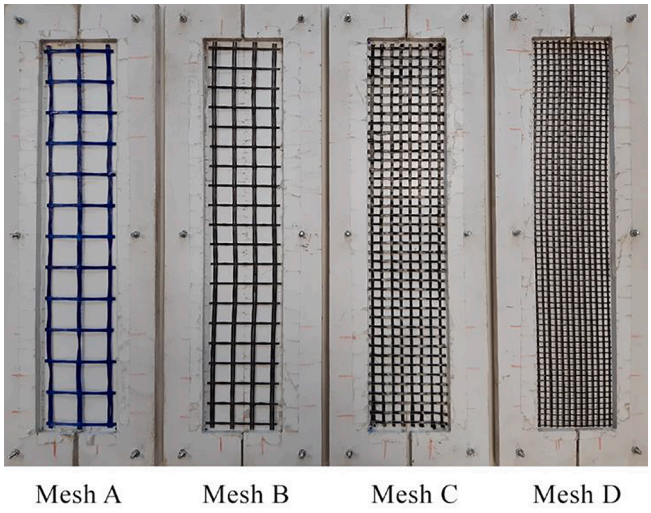

Fig. 2. Production of TRM specimens.

Table 2
Experimental program summary.

Set	Mesh	Mortar	Temperature exposure (°C)	Samples
A20	A	M1	20	4
A100			100	4
A200			200	4
A400			400	4
A600			600	4
B20	B	M2	20	4
B100			100	4
B200			200	4
B400			400	4
B600			600	4
C20	C	M2	20	4
C100			100	4
C200			200	4
C400			400	4
C600			600	4
D20	D	M2	20	4
D100			100	4
D200			200	4
D400			400	4
D600			600	4

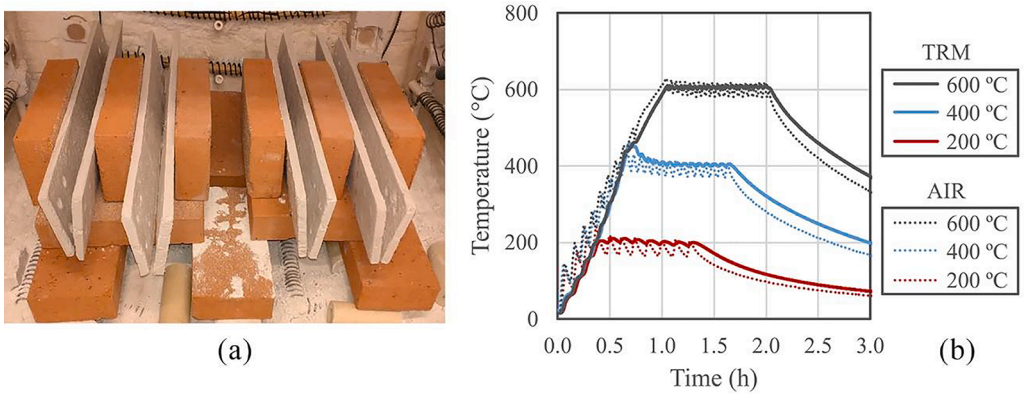

Fig. 3. Temperature exposure: (a) detail of specimen arrangement inside the furnace; (b) temperature curves recorded by thermocouples for the 200, 400 and 600 °C cycles.

of 15 MPa for both mortars and a modulus of elasticity of 10 GPa (M1) and 8 GPa (M2), after 28 days.

The textile reinforced mortar (TRM) specimens were designed according to the recommendations of AC434 [19] and RILEM TC 232-TDT [20] and were manufactured in individual removable molds, as shown in Fig. 2. The specimens were prismatic in shape, with a length of 500 mm, a width of 100 mm and a thickness of 10 mm. The indicated length was established to define an anchorage zone of 100 mm at both ends and to maintain a central measuring zone of 300 mm. The width was defined to accommodate at least three fiber bundles for the mesh with the largest size (mesh A). The manufacturing process basically consisted of three stages: (i) placement of a first layer of mortar 4 or 5 mm thick uniformly distributed over the mold; (ii) placement of the mesh, applying a slight pressure and taking care that the fibers were perfectly aligned and symmetrically centered in the mold; (iii) placement of the second layer of mortar and flush with the upper face of the mold with the help of a metal spatula. In all cases a single layer of reinforcement was used and, of the four different fabrics used, only mesh C was pre-impregnated before placement with the liquid phase of mortar M2, in order to improve its bonding, and in accordance with the manufacturer's recommendations. All specimens were demolded 48 h after fabrication and cured at laboratory ambient conditions for 90 days before testing.

2.2. Experimental campaign and temperature exposure

A total of four TRM reinforcement systems have been studied. For each TRM system, 20 specimens (coupons) were produced, so that they could subsequently be damaged at different temperature levels. Table 2 summarizes the characteristics of all the series and the nomenclature adopted: the first letter indicates the type of mesh (A, B, C and D) and then the exposure temperature level is defined (20, 100, 200, 400 and 600 °C). Each series consists of four specimens, so the total number of specimens manufactured is 80. Note that mesh A is applied with mortar M1, while meshes B, C and D are combined with mortar M2.

The heat treatment was carried out in a programmable electric furnace in batches of 8 specimens, as can be seen in Fig. 3(a), which shows a detail of the arrangement of the specimens inside, supported by refractory ceramic bricks. Heating was carried out at a constant rate of 10 °C/min until the target temperature (100, 200, 400 or 600 °C) was reached, and maintained for one hour. The furnace was then switched off and the specimens were cooled slowly for 24 h until they reached approximately the ambient temperature of the laboratory. Various tests had been carried out previously, measuring with thermocouples the temperatures of the air inside the oven and also inside the coupons. For this purpose, some sample specimens were drilled and thermocouples were installed inside, which were subsequently sealed with refractory mastic. Fig. 3(b) shows both temperature curves for the 200, 400 and 600 °C cycles. As can be seen, the differences at each temperature level are negligible, given the reduced thickness of the coupons. All the tests performed, as will be specified below, were carried out within a period not exceeding 24 h after removal of the specimens from the furnace, in order to minimize the risk of deterioration (especially in the specimens exposed to 400 and 600 °C, which exhibited serious damage as will be justified in Section 3).

2.3. Non-destructive tests

Non-destructive testing enables estimation of the mechanical properties of construction materials without the need to extract specimens in situ, an aspect of vital importance when working, for example, in

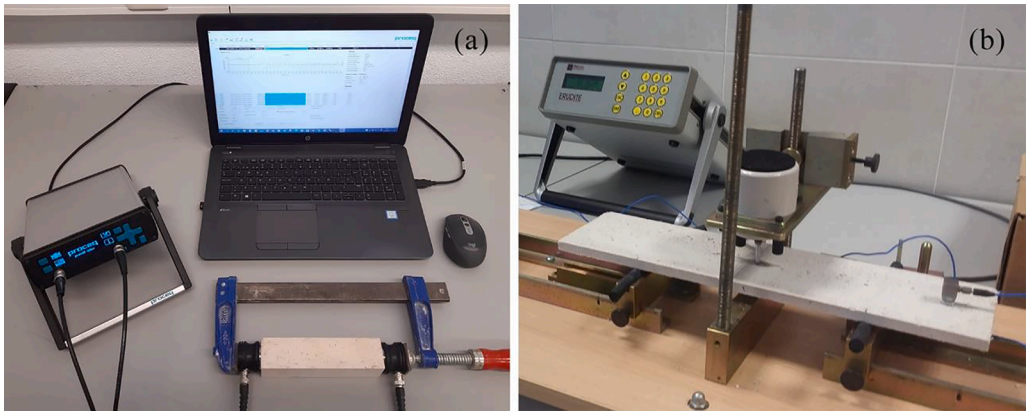

Fig. 4. Non-destructive tests set-ups: (a) measurement of ultrasonic wave propagation on mortar samples; (b) sonic resonance tests on TRM coupons.

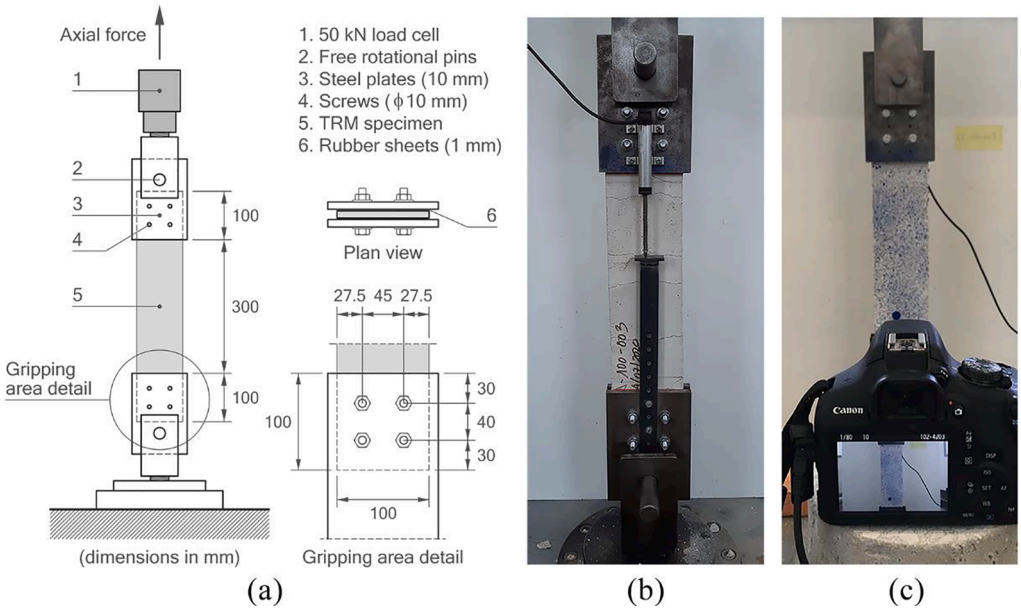

Fig. 5. TRM tensile test set-up: (a) schematic view; (b) LVDT arrangement; (c) DIC monitoring.

buildings of historical or architectural value where this is generally not possible. In this research, two types of non-destructive tests have been performed to determine the dynamic moduli of elasticity (E_{dyn}) of mortars and TRM coupons, before and after exposure to the different temperature levels indicated above (Table 2).

On the one hand, 15 prismatic specimens of 160 × 40 × 40 mm^3 were prepared with both mortars used (M1 and M2), divided into series of three specimens for each temperature level. The mortars were cured in ambient laboratory conditions for 90 days before testing. The mortar specimens were subjected to ultrasonic wave propagation tests according to ASTM D2845-08 [44], for which a Proceq Pundit Lab + equipment connected to a computer was used for data acquisition and processing. Obtaining the dynamic modulus from this test implies the knowledge of the real density of the mortar, so each mortar specimen was weighed on a high precision balance to obtain these data. The tests were performed along the axial direction of the specimens and an ultrasonic couplant and a steel clamp were used to enhance sound transmission, as shown in Fig. 4(a). Once the velocities of the compression (V_p) and shear (V_s) waves were determined, the dynamic elastic modulus was easily obtained from Eq. (1), where ρ is the density of the mortar.

$$E_{dyn} = \frac{\rho V_s^2 \left(3V_p^2 - 4V_s^2\right)}{V_p^2 - V_s^2} \quad (1)$$

On the other hand, in all the TRM specimens (see Table 2), the fundamental bending resonance frequency was determined according to ASTM E1875-20a [45], before and after exposure to the different temperature levels. Fig. 4(b) shows the general test setup, with the specimen simply supported on two elastomers arranged at a distance of 0.224 times the length of the piece, measured from both ends. The Erudite MKIV (PC1004) analyzer was used as excitation equipment, acting on the center of the specimen. A PCB 333B50 accelerometer with 1 V/g sensitivity, placed at one end of the specimen, as well as a Kyowa PCD-320 acquisition system and a PCB 482A22 signal conditioner were used as recording system. Once the fundamental bending resonance frequency (f_f) was determined, and knowing the length (L), thickness (t), width (b) and mass (m) of the specimen, the value of the dynamic modulus of elasticity was obtained by means of Eq. (2).

$$E_{dyn} = 0.9465\left(\frac{m \cdot f_f^2}{b}\right)\left(\frac{L^3}{t^3}\right)\left[1 + 6.585\left(\frac{t}{L}\right)^2\right] \quad (2)$$

2.4. Destructive tests

The same 160 × 40 × 40 mm^3 mortar specimens that had been subjected to the ultrasonic test -as explained in the previous point- were tested immediately afterwards in flexure and compression according to UNE-EN 1015-11:2020 [46]. For the bending test, a press equipped with a 20 kN load cell was used, placing the specimens on two steel rollers 100 mm apart and applying the load in the center of the specimen at a constant speed of 30 N/s. The maximum load applied was recorded, with which the bending strength was determined as the average of the 3 specimens that make up each of the series tested. With the two resulting halves of each specimen, the compressive strength was determined, for which another testing machine equipped with a 200 kN load cell was used. For the compression test, two 40 × 40 mm^2 support plates were used. On this occasion, the load was applied at a constant speed of 250 N/s, which was reduced to 100 N/s in the case of the series that had been previously subjected to temperature levels of 400 and 600 °C. Finally, the compressive strength was obtained as the average value of the 6 fragments tested in each series.

Likewise, the same TRM coupons that had previously tested by non-destructive testing to determine the flexural resonance frequency were now tested in uniaxial tension following the indications of the AC434 [19] and RILEM TC 232-TDT [20] guides. As will be justified in Section 3, mortars were seriously damaged after exposure to certain temperature levels, so that the anchorage of the pieces presented some difficulty (especially in the series subjected to temperature levels above 400 °C). For this reason, and based on different tests previously carried out [5,6,29], it was decided to increase the anchorage capacity by means of 4 holes drilled at both ends of the pieces and the placement of 4 screws of 10 mm in diameter, as shown in Fig. 5(a). The specimens were placed between two 10 mm thick steel plates, with an intermediate sheet of elastic material 1 mm thick to improve the contact between the two materials and to evenly distribute the pressure exerted by the screws. Although the method of anchorage by direct screwing through the TRM coupons is not contemplated in the aforementioned guides, it has proved to be totally satisfactory; in no case did the specimens break as a result of the drill holes and no failures were detected in the anchorages in any of the series studied. A press equipped with a 50 kN load cell was used for the test and the anchorage device was designed to allow free rotation in the plane of the specimen and at both ends, in order to correct possible

Table 3
Dynamic elastic modulus, E_{dyn} (in MPa) in mortars and TRM series (coefficient of variation expressed as percentage in parentheses).

Exposure temperature (°C)	Mortar [a]		TRM [b]			
	M1	M2	A	B	C	D
20	10263 (2.2 %)	8566 (4.5 %)	8850 (2.1 %)	6546 (16.1 %)	6223 (17.2 %)	5703 (5.6 %)
100	9109 (0.9 %)	8113 (0.6 %)	8630 (7.2 %)	5935 (11.8 %)	5528 (5.2 %)	5162 (17.7 %)
200	8288 (1.9 %)	6864 (3.5 %)	6791 (25.7 %)	3620 (13.5 %)	3860 (24.8 %)	3782 (14.9 %)
400	6532 (1.9 %)	3787 (4.4 %)	6421 (9.2 %)	2573 (9.8 %)	2428 (15.5 %)	2390 (13.8 %)
600	3686 (1.0 %)	1507 (6.6 %)	4852 (3.9 %)	1121 (9.7 %)	1393 (9.2 %)	1183 (19.0 %)

[a] E_{dyn} from ultrasonic tests in 160x40x40 mm^3 mortar samples.
[b] E_{dyn} from sonic resonance tests in TRM specimens.

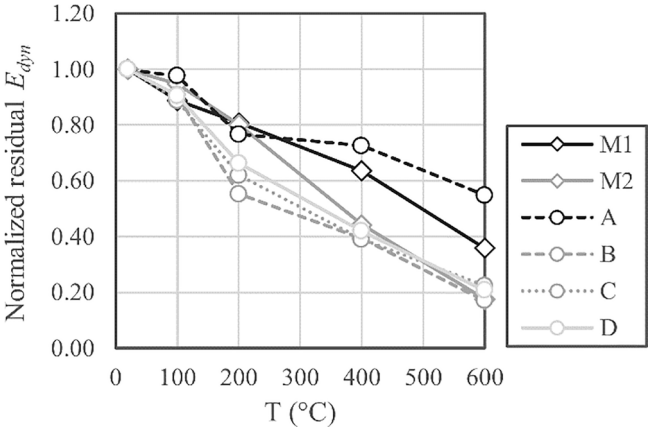

Fig. 6. Evolution of the dynamic modulus of elasticity with temperature (normalized residual values).

eccentricities or errors in centering.

The load was applied by displacement control, with a constant value of 0.2 mm/min until failure. Two different methods were used to control the deformations: (i) on one side of the specimen, Fig. 5(b), an LVDT was placed directly anchored to the steel plates at both ends -with an initial measurement length of 300 mm- and connected to an HBK QuantumX MX1615B data acquisition system, programmed at a sampling rate of 1 Hz; (ii) the opposite side, Fig. 5(c), was monitored by Digital Image Correlation (DIC), for which a camera with a resolution of 16 MP was installed at 75 cm from the specimen, applying a stochastic paint spray pattern (speckle) on the mortar surface to improve the contrast and the subsequent analysis process, which was carried out using the GOM Correlate software [29].

3. Results and discussion

3.1. Effect of temperature on dynamic modulus of elasticity

The dynamic moduli of elasticity (E_{dyn}) obtained experimentally in the two types of mortars used and also in the four different combinations of TRM specimens are summarized in Table 3. These results, based on non-destructive testing, also show the impact of the different exposure temperatures considered. The corresponding coefficients of variation are also included, in all cases. In addition, Fig. 6 graphically represents

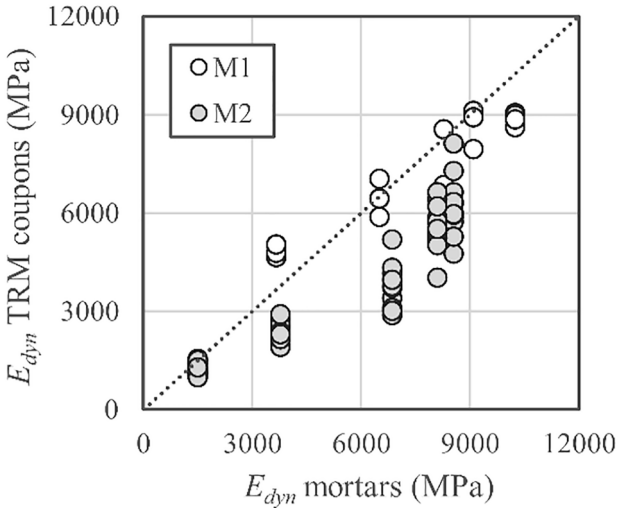

Fig. 7. Relationship between dynamic elastic modulus obtained from ultrasonic tests in mortar samples (X-axis) and sonic resonance tests in TRM specimens (Y-axis).

the normalized residual values, i.e. the ratio between the modulus at a given temperature ($E_{dyn(T)}$) with respect to that of the same series at room temperature ($E_{dyn(20)}$).

Regarding the results of the mortars studied, it can be observed, firstly, that the experimental results for both mortars at room temperature are very similar to the values provided by the manufacturer (10000 MPa for mortar M1 and 8000 MPa for M2). Secondly, it is important to emphasize that the coefficients of variation obtained for each series are considerably small, which shows the homogeneity and validity of the tests. In the light of the results shown, the temperature exposure produced notable decreases in the dynamic modulus of elasticity of both mortars: in the case of M1, reductions of around 40% at 400 °C and 60% at 600 °C were observed; in the case of M2, the drops were considerably steeper, of around 60% at 400 °C, and even up to 80% at 600 °C. Therefore, it seems evident that the matrix was seriously damaged as a consequence of exposure to high temperatures.

With respect to the TRM coupons, the type of fabric -fiber type or mesh pitch- did not seem to have any influence on the results, i.e., E_{dyn} seems to depend only on the characteristics of the matrix mortar. Curves B, C and D in Fig. 6 describe the same downward trajectory as the exposure temperature increased. In general, the method of estimating the dynamic modulus by bending resonance on TRM coupons provided appreciably lower values with respect to the results obtained by ultrasound on mortar specimens. However, in terms of the decrease in E_{dyn} as a consequence of temperature, it can be seen that the series

Table 4
Compressive and flexural strengths in 160 × 40 × 40 mm^3 mortar samples (coefficient of variation expressed as percentage in parentheses).

Exposure temperature (°C)	M1		M2	
	Compressive strength (MPa)	Flexural strength (MPa)	Compressive strength (MPa)	Flexural strength (MPa)
20	9.55 (15.9 %)	4.03 (10.7 %)	16.93 (5.4 %)	5.28 (13.3 %)
100	8.33 (22.5 %)	3.32 (29.0 %)	16.80 (4.0 %)	6.16 (9.0 %)
200	8.38 (16.3 %)	3.10 (4.1 %)	15.68 (20.7 %)	5.49 (11.9 %)
400	8.79 (17.1 %)	2.93 (6.8 %)	7.14 (12.1 %)	2.42 (9.9 %)
600	4.47 (9.8 %)	0.73 (7.3 %)	5.16 (6.5 %)	1.45 (8.4 %)

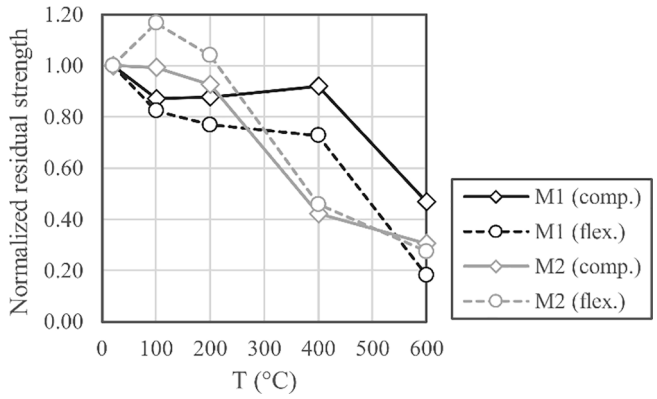

Fig. 8. Evolution of the compressive and flexural strength with temperature (normalized residual values).

manufactured with M2 mortar (series B, C and D) suffered almost identical losses, and only in series A (manufactured with M1 mortar) lower decreases were obtained, of approximately 25% at 400 °C and 45% at 600 °C. Finally, Fig. 7 shows the relationship between the dynamic moduli of elasticity obtained in the mortar specimens (on the X-axis) and in the TRM coupons (on the Y-axis) for all the temperature levels studied. The results are now grouped according to the two types of mortar used since, as has been shown, the type of mesh did not produce substantial differences. It can be seen that both methods provided similar results in the case of M1 mortar, although the estimation of E_{dyn} by bending resonance clearly gave lower values for the series manufactured with M2 mortar.

3.2. Effect of temperature on mortar strengths

The results for the compression and 3-point-bending tests on the 160 × 40 × 40 mm^3 mortar specimens are summarized in Table 4, according to the different exposure temperature levels, including the corresponding coefficients of variation, for each type of mortar and temperature level studied. The residual values are plotted in Fig. 8, so as to be able to easily appreciate the loss of mechanical capacity of each mortar as a function of temperature.

The results show that, at room temperature, the compressive strength of M2 mortar matched the manufacturer's specifications (≥15 N/mm^2), although this was not the case for M1, whose strength did not reach 10 N/mm^2. It is clearly observed how M1 maintained its properties relatively constant up to 400 °C, although the flexural strength (whose loss was estimated to be around 25%) deteriorated to a greater extent than the compressive strength (less than 10%). However, a serious degradation is observed at 600 °C (about 50% in compressive strength and 80% in flexural strength). In the case of M2, however, the strength degradation was remarkable from 200 °C upwards, and both were reduced by approximately 70% at 600 °C. It is interesting to compare these results with the decreases obtained in the dynamic modulus of elasticity in both mortar specimens and TRM coupons (Figs. 6 and 8). It becomes clear that in the case of M2 mortar, the percentage drops at 400 and 600 °C were virtually identical, with slight differences being observed in the case of M1 mortar. In view of the results, it can be seen that mortar M1 presented greater stability when exposed to high temperatures, although both mortars underwent significant degradation at levels of 600 °C, which would arguably correspond to the action of a high intensity fire acting directly on the reinforcing materials. It can therefore be concluded that the application of non-destructive testing methods for the evaluation of damage due to high temperatures in this type of materials is quite acceptable, which implies an attractive solution in the case of interventions in those buildings where, for whatever reason, it would not be possible to extract specimens on site.

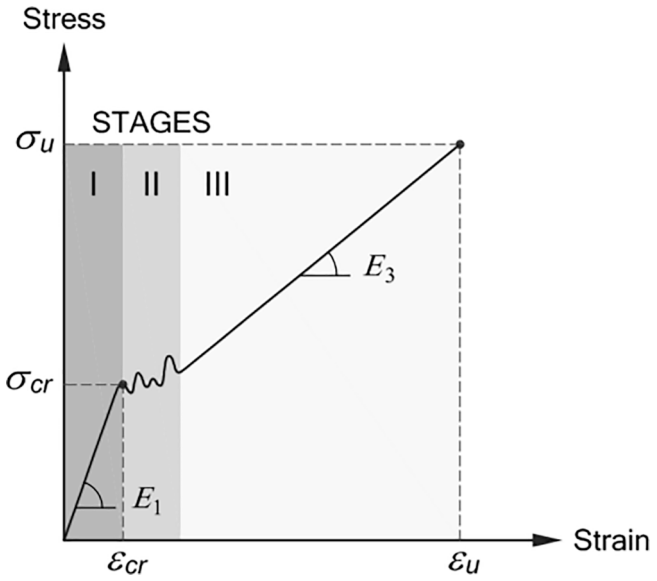

Fig. 9. Idealized stress-strain TRM response.

3.3. Effect of temperature on TRM: stress-strain response

For the interpretation of the results of uniaxial tensile tests on TRMs, an idealized stress-strain curve is represented in Fig. 9 with the three characteristic phases with which this type of material normally responds, as explained in Section 1: I (uncracked stage), II (crack development) and III (cracked stage); however, it should be pointed out that these three stages cannot be clearly differentiated in all cases, as will be justified later on. This curve makes it possible to identify the fundamental parameters of the test: stress (σ_{cr}) and strain (ε_{cr}) at the point where the mortar matrix cracks; modulus of elasticity of the uncracked TRM (E_1); stress (σ_u) and strain (ε_u) at failure; and modulus of elasticity of the cracked TRM (E_3). With respect to the failure modes, it is important to note that in some series, failure was reached by fiber rupture, which translated into a clearly defined point in the stress-strain diagram. However, in other cases, failure occurred by slippage of the fibers with respect to the mortar matrix, obtaining an approximately horizontal branch where the strains increased at more or less constant stress; in these cases, the determination of the ultimate strain was not as immediately apparent.

The stress-strain curves obtained experimentally are shown in Fig. 10 where, depending on the type of mesh, the average curve of the 4 specimens that make up each series is given for the 5 exposure temperature levels. To facilitate the reading of the article, it has been decided to separate in Appendix A the detailed curves of the 20 series tested. These graphs provide the average and bilateral 90% confidence interval of the stress-strain relationship. Table 5 summarizes the results obtained, expressing the stresses and moduli of elasticity with respect to the area of the fibers, adopting the values provided by the manufacturer for each type of mesh (Table 1). Furthermore, the maximum stress of phase I with respect to the gross section of the mortar matrix ($\sigma_{cr,m}$) is also provided, in order to compare these values with the corresponding flexural strengths (Table 4). To assist in the interpretation of the results in Table 5, it has been decided not to include the coefficients of variation, since it is considered that the confidence intervals defined graphically in the curves of Appendix A allow a clearer appreciation of the dispersions obtained in each series and in each phase of the test.

The results show, in general terms, that the response of the TRM at room temperature or at moderate exposure levels (up to 200 °C) was different depending on the type of reinforcing mesh and the mortar used. In the case of A-series, stage II segued into stage III without any clear transition point between the two. Failure generally occurred by slippage

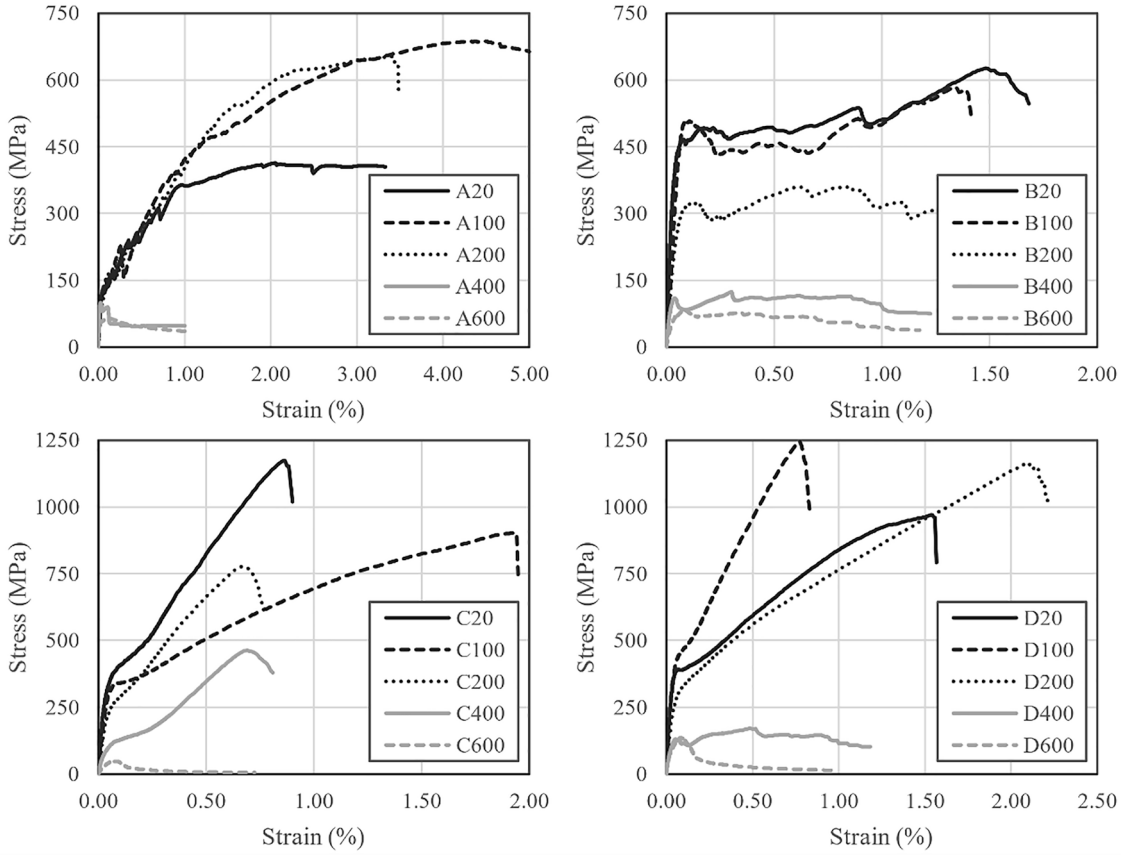

Fig. 10. Experimental results on TRM tensile tests (average stress-strain curves for 4 samples per set).

Table 5
Experimental results on TRM tensile tests.

Set	σ_{cr} (MPa)	$\sigma_{cr,m}$ (MPa)	ε_{cr} (%)	E_1 (GPa)	σ_u (MPa)	ε_u (%)	E_3 (GPa)
A20	128	0.91	0.056	428	413	2.050	27.2
A100	125	0.89	0.042	504	687	4.483	29.8
A200	79	0.56	0.031	360	652	3.417	29.1
A400	99	0.70	0.023	247	90	0.103	0
A600	61	0.43	0.016	190	64	0.121	0
B20	466	1.65	0.073	1371	627	1.483	24.9
B100	505	1.78	0.085	790	585	1.342	21.7
B200	302	1.07	0.073	657	354	0.883	22.2
B400	109	0.39	0.037	496	114	0.850	19.7
B600	83	0.29	0.080	230	68	0.617	4.3
C20	375	1.80	0.067	1104	1174	0.867	111.4
C100	338	1.62	0.080	845	904	1.933	40.5
C200	258	1.24	0.065	646	778	0.667	98.7
C400	120	0.58	0.073	334	463	0.692	74.3
C600	48	0.23	0.063	120	48	0.063	0
D20	391	1.52	0.062	1221	970	1.533	54.1
D100	445	1.73	0.072	1171	1246	0.775	126.9
D200	306	1.19	0.073	764	1165	2.100	37.6
D400	131	0.51	0.053	435	171	0.483	11.7
D600	136	0.53	0.085	377	136	0.085	0

of the fibers inside the mortar matrix, which resulted in a last branch with a gentle slope in which it was not possible to establish a specific point of failure in all cases. In B-series, stages II and III appeared to combine in a single, relatively horizontal branch, in which slight stress drops were appreciated as the mortar matrix cracked. Failure in this case occurred by fiber rupture, so the ultimate stress could be identified relatively easily. With respect to C and D-series, bilinear behavior was characterized by the absence of stage II and a well-defined failure point as a consequence of fiber rupture. In general, the observed responses were consistent with those described in other investigations [25]. With respect to the dispersions obtained, it can be seen from the curves in Appendix A how the TRMs with the glass fiber meshes (A and B-series) presented the widest confidence intervals, while the series with the carbon and basalt fiber meshes (C and D-series) responded in a much more homogeneous way, with very narrow confidence intervals.

Analyzing the specific values, and always at room temperature, it can be seen that the fiber cracking stress was not reached in any case, obtaining σ_u values of 26% (set A20), 49% (set B20), 23% (set C20) and 63% (set D20), with respect to the data provided by the manufacturer for bare meshes (Table 1). With regard to cracking stress of the mortar, the resulting $\sigma_{cr,m}$ values were clearly smaller than those obtained in the flexural tests in the corresponding matrices (Table 4): 23% (set A20 vs. mortar M1) and 29% to 34% (sets B20, C20 and D20 vs. mortar M2). In terms of the modulus of elasticity, the comparison between E_3 and the information provided by the manufacturer for the different meshes is relevant (Table 1). The moduli in the TRMs were again found to be lower: 82% (set A20), 35% (set B20), 44% (set C20) and 61% (set D20). The results, in general, are consistent with those reported in other experimental campaigns with glass [22], carbon [21] or basalt [23] meshes.

From the point of view of the influence of temperature on the TRM, it can be observed that, in general terms (Fig. 10), the 4 materials studied performed well up to exposure levels of 200 °C, suffering significant losses in mechanical capacity at 400 °C and above. In A-series, it can be seen that temperatures of 100 and 200 °C clearly improved the behavior of the TRM. This effect has also been observed in other previous investigations [34–36,41,42] and is essentially attributed to two reasons: (i) during the cooling process that follows the thermal treatment, a shrinkage of the mortar matrix occurs that improves the adhesion with the fibers, an effect that is increased as the water contained in the material evaporates; (ii) at these temperature levels it has been found that

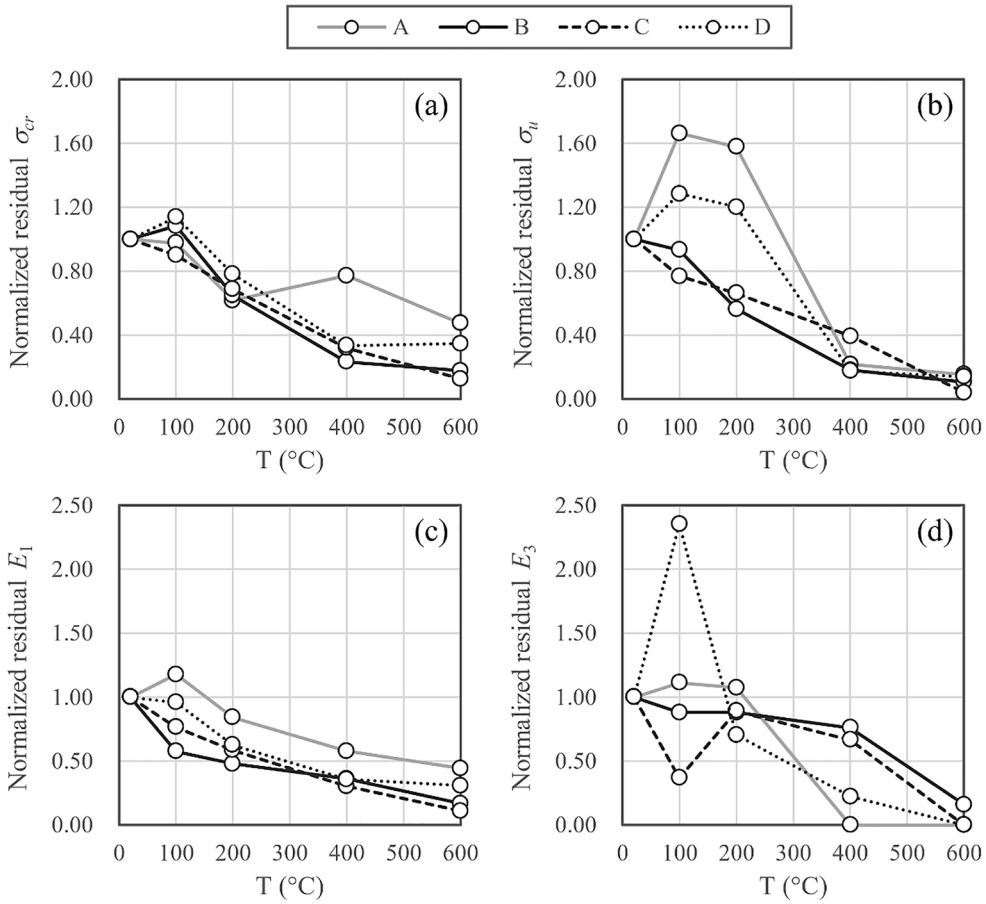

Fig. 11. Evolution of TRM properties with temperature: (a) matrix cracking tensile stress; (b) ultimate tensile stress; (c) uncracked elastic modulus; (d) cracked elastic modulus. Normalized residual values in all cases.

some polymers with which the meshes are coated change from visco-elastic to plastic state with heat, recovering their original state upon cooling, a process that improves the adhesion between the fibers and the matrix. For temperatures of 400 °C and above, and despite the fact that the M1 mortar maintained its properties relatively intact (Table 4), it was observed how the TRM lost all its mechanical capacity as a consequence of the degradation of the mesh, as will be analyzed in the following section.

B-series did not show any improvement in its behavior as a consequence of temperature, and it was found that the material remained intact at 100 °C, detecting the first signs of deterioration at 200 °C and obtaining significant drops over 400 °C, the temperature at which degradation of the M2 mortar occurs (Table 4). The failure of the TRM at these temperature ranges was again attributed to the degradation of the mesh, although in this case the deterioration of the mortar also had an influence, causing the transfer of stresses between the different fibers to lose effectiveness, so that a localized breakage of some fibers quickly led to the failure of the composite.

In C-series, no improvement is observed after the increase in temperature either. On the other hand, among the 4 meshes studied, it is only in this case that the material retains a certain mechanical capacity up to 400 °C, becoming completely damaged at 600 °C. The explanation is attributed to the fact that the carbon fiber meshes are the only ones that are not polymer-coated and are only pre-impregnated with the liquid phase of the M2 mortar during the execution of the coupons. The decomposition of the mesh coating polymers at temperature levels of 400 °C has been shown to have a decisive influence on the strength of TRMs as the bond between the fibers and the mortar matrix disappears [35].

Finally, in D-series a clear increase in the mechanical capacity at 100 and 200 °C was again observed, in a similar way as discussed above for A-series. On the other hand, the increase in stiffness experienced by the material in the samples exposed to 100 °C was remarkable, with the modulus E_3 being superior to the value provided by the manufacturer for the corresponding mesh (Table 1). This increase has already been reported in some previous investigations [22,30] and is basically attributed to the fact that the mortar matrix can provide additional stiffness in certain cases, in addition to allowing a much more homogeneous distribution of stresses between the fibers with respect to the tensile test of dry meshes, where irregular distributions or stress concentrations may occur in the anchorage zones. Once again, it is observed that, at 400 °C and above, the material was badly damaged as a consequence of the degradation of the mesh and the M2 mortar, in a very similar way to that explained in the case of the B-series.

To analyze the degradation of the mechanical properties of the TRMs after being damaged at different temperature levels, Fig. 11 presents the reductions obtained in the mortar matrix cracking strength (Fig. 11(a)), ultimate strength (Fig. 11(b)), modulus of elasticity of the uncracked TRM (Fig. 11(c)) and modulus of elasticity of the cracked TRM (Fig. 11 (d)). In all cases, the normalized residual values are plotted, i.e., the ratio of the result at a given temperature to the equivalent series at room temperature. It can be seen, first of all, that the evolution of σ_{cr} depended fundamentally on the type of mortar used, showing that in A-series (mortar M1) better results were obtained than in B, C and D-series (mortar M2), where the decreases at 400 and 600 °C were quite marked. The results are consistent with those presented previously for both mortars (Fig. 8), noting, in general, what has already been observed in Section 3.2, where M1 retains its properties relatively well up to 400 °C,

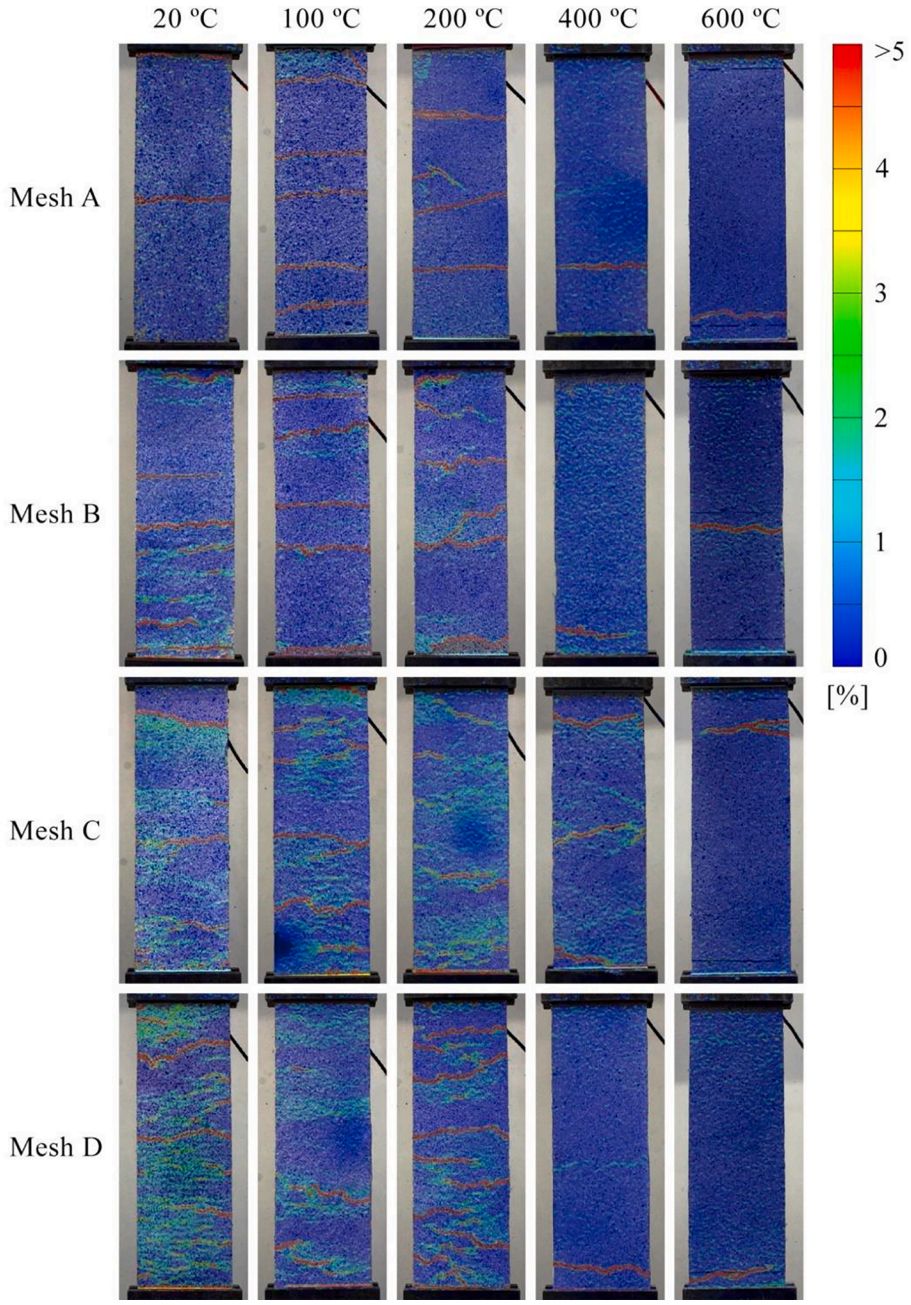

Fig. 12. Crack patterns in all series obtained by DIC analysis.

unlike M2, which suffers a significant decrease from 200 °C onwards. A possible explanation for this behavior is that M2 mortar is marketed as a high ductility mortar, so its dosage incorporates synthetic polymers in aqueous dispersion, which are strongly degraded at temperatures not higher than 200 °C. Another aspect that may affect the different behavior between M1 and M2 is that the fibers contained in M2 mortar are affected by temperature, reducing the tensile strength of the matrix.

Regarding the ultimate stress (σ_u), it should be noted that the underlying factor responsible for reaching this parameter is the type of fabric, so that the evolution of this parameter is strongly conditioned by the meshes used. In A and D-series, the increase in resistance at temperatures of 100 and 200 °C was noteworthy, the possible explanation for which has been discussed above. On the other hand, B and C-series did not experience this improvement, obtaining approximately linear resistance losses with increasing temperature. It was observed in all cases that the material was heavily damaged at 400 °C and practically unusable at 600 °C, as a consequence of the degradation of the meshes and as will be justified in the following section.

From the point of view of the modulus of elasticity, it can be seen how the decreases in E_1 were also practically linear as the temperature increased, and only in the case of the A-series was a slight improvement detected at 100 °C. The results are comparable with the dynamic moduli of elasticity obtained for mortars (Fig. 6), which again shows that nondestructive testing can be of great interest for evaluating the loss of mechanical capacity of this type of material without the need to extract samples on site.

Finally, greater differences are observed in the evolution of E_3 with temperature, the increase in D-series at 100 °C being particularly striking. The possible reasons for this increase have been explained above. While B and C-series appear to retain their stiffness up to 400 °C, in A and D-series there are very important reductions at this temperature level, with all series being severely damaged at 600 °C.

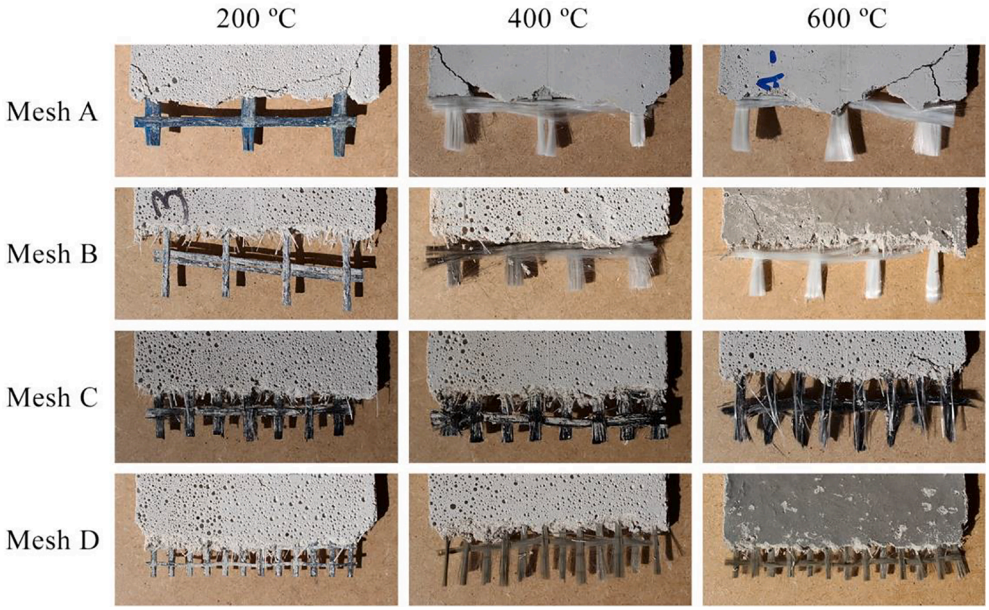

Fig. 13. Detail of TRM coupons degradation for 200, 400 and 600 °C.

3.4. Effect of temperature on TRM: crack patterns and failure modes

To study the cracking patterns, Fig. 12 displays the results of the analysis by Digital Image Correlation (DIC), taking a representative specimen from each of the sets tested. The images correspond to the failure point (σ_u) and have been processed using the GOM Correlate software [29]. The strains are indicated with a color code where red represents values above 5%, which occur in the vicinity of the main cracks. In general, it is evident that cracking patterns vary significantly among the different materials studied and also with the exposure temperature.

In the case of A-series, at room temperature a single crack was produced in the central zone of the specimen, although in other cases it was concentrated in the area near the anchor plates. From this point on, the mesh slipped with respect to the mortar matrix without new cracks being detected. At 100 and 200 °C a greater distribution of cracking along the piece was observed, and also notable increases in the ultimate strength, in line with the improvement of bonding between the fabric and the mortar as discussed in the previous section. At 400 °C and above, cracking was again concentrated in a single section, usually at the ends of the specimens. At these temperature levels, the mesh was heavily degraded, and failure occurred immediately after matrix rupture.

The response of B-series was different, showing that at room temperature the distance between cracks corresponded approximately to the size of the reinforcing mesh (25 mm, Table 1). At 100 and 200 °C, the separation between cracks widened, which indicates a gradual loss of bond between the mesh and the mortar. Thus, no improvement in the behavior of the TRM was observed as in the previous case. Again at 400 °C there was a dramatic drop in strength, with both matrix and mesh strongly degraded. A single crack was then produced in the vicinity of the anchor plates or in the central zone of the specimen.

Mesh C, as discussed in the previous section, is the only one that maintained a certain mechanical capacity up to 400 °C, as can be clearly seen in the cracking pattern. Meanwhile, at temperatures from 20 to 200 °C, no substantial differences were observed, with a fairly homogeneous distribution of cracks along the entire piece. At 600 °C, and with the mesh and matrix completely degraded, failure occurred at very low tensile stresses, with a single crack generally concentrated at the ends of the specimens.

Finally, in the case of mesh D, at room temperature the distance between cracks was found to be very small, since it was fundamentally conditioned by the size of the reinforcing mesh (6 mm, Table 1). Between 100 and 200 °C there were no significant differences, obtaining a homogeneous distribution throughout the piece. Again, it was at 400 °C, as in meshes A and B, that a sharp drop in strength was observed, with a single clearly marked crack in the vicinity of the anchorage zones.

Overall, the results obtained are similar to those reported by Rambo et al. [37], the only published research in which the behavior of TRM exposed to elevated temperatures has been analyzed by means of DIC. In this work, it was found that at 400 °C the failure modes were drastically modified as a consequence, basically, of the degradation of the mortar matrix and the decomposition of the coating polymers of the reinforcement meshes, losing the bonding capacity between both materials.

In order to analyze the degradation of the meshes as a consequence of exposure to temperature, Fig. 13 shows a detail of the TRMs tested, in which part of the mortar matrix has been removed to expose the fibers. Only the series subjected to 200, 400 and 600 °C are presented, since at lower temperatures the materials remained virtually intact, and no alteration was detected as a consequence of the exposure to heat. From the visual inspection carried out, the meshes did not show any noticeable signs of deterioration at temperatures up to 200 °C. However, it is clearly observed that at 400 °C the coating polymer of meshes A, B and D was completely decomposed, leaving the fibers loose and without any capacity to adhere to the mortar matrix. This is arguably the main cause of the significant strength losses discussed in the previous section. Regarding mesh C, it should be remembered that it is the only one of the four that is not polymer-coated. Although certain symptoms of deterioration are observed in the carbon fibers and the mortar matrix is seriously damaged at this temperature level, the TRMs of this series still retained certain mechanical capacity, since they did not suffer the adhesion problem that arose with the rest of the meshes. Finally, at 600 °C the fibers appeared seriously worn out in all cases, and the mechanical properties of the material were completely lost. It is worth mentioning, on the one hand, that the fibers contained in the composition of mortar M2 (meshes B, C and D) also underwent significant degradation at 400 °C and above, as shown in the images. Additionally, it should be pointed out that the M2 mortar has synthetic polymers in its dosage, which are vulnerable to exposure to temperatures not exceeding 200 °C. This could be one of the causes of the significant drops in the matrix cracking strength (σ_{cr}) that have been explained above (Fig. 11 (a)).

Table 6
Experimental campaigns in other studies.

Ref.	Authors	Textiles	Mortar matrix	Temperature exposure (°C)
1	Colombo et al.	Glass	High strength mortar	20-200-400-600
2a	De Andrade et al.	Carbon (uncoated)	Cementitious	20-100-150-200-400-600
2b	De Andrade et al.	Carbon (coated)	Cementitious	20-75-150-200-300-400-600-1000
3	Rambo et al.	Basalt	Cementitious	20-75-150-200-300-400-600-1000
4a	Messori et al.	Glass (coating 1)	Hydraulic lime	20-100-150-200-250
4b	Messori et al.	Glass (coating 2)	Hydraulic lime	20-100-150-200-250
5	Tlaiji et al.	Glass	Cementitious	20-75-150-300-400-600
6	Homoro et al.	Glass	Cementitious	20-75-150-300-400-600

3.5. Effect of temperature on TRM: comparison with other studies

To conclude the discussion, it is considered appropriate to compare the results obtained with those reported in previous investigations. It is worth remembering that the studies published to date are scarce, so the information available is limited. To establish the comparisons, the works of Colombo et al. [34], De Andrade et al. [35], Rambo et al. [36], Messori et al. [39], Tlaiji et al. [41] and Homoro et al. [42] have been selected, whose main conclusions have been pointed out in Section 1. Nevertheless, the main characteristics of the experimental campaigns proposed in these works are summarized in Table 6.

The comparison of the results is proposed in terms of the TRM ultimate strength (σ_u). For this purpose, Fig. 14 shows the losses obtained in the 4 series tested (A, B, C and D) together with those reported in the aforementioned works, for the different levels of exposure temperature. First of all, a more than acceptable homogeneity should be noted, taking into account the dispersions presented in this type of tests and the large number of variables that can influence the results. However, it is necessary to highlight that in A-series a notable deviation is observed with respect to the rest, corresponding to the important improvements in resistance detected at 100 and 200 °C, as discussed above. In most cases, it is observed that the TRMs maintained (or even improved) their mechanical capacity at moderate exposure levels (up to 200 °C), for the reasons explained in Section 3.3. From this point on, more or less significant decreases in resistance occur up to 400 °C, which correspond to the degradation of the mortar matrix and the reinforcement meshes and, most particularly, to the decomposition of the fiber coating polymers, seriously compromising the adhesion between both materials. In this sense, it should be useful to observe the curve (2a) reported by De Andrade et al. for the case of uncoated carbon fiber fabrics, where this problem does not occur. Finally, it is evident how these types of materials are profoundly damaged at 600 °C, suffering resistance drops of more than 80% in most cases. At this temperature level, it has been found that the reinforcement polymer fabrics of the TRM become considerably degraded, so that failure occurs at very low stresses once cracking of the mortar matrix is initiated.

4. Conclusions

In this work, the tensile behavior of TRM specimens produced with 4 types of fabrics (two glass, one carbon and one basalt fiber meshes) and 2 different limed-based mortars, has been analyzed. The samples were exposed to different temperatures levels (up to 600 °C). The materials have been subjected to both non-destructive and destructive tests, in order to determine their mechanical properties. The main conclusions derived from this research can be summarized in the following points:

- The evaluation of the dynamic elastic modulus by non-destructive tests (ultrasonic wave propagation on mortar specimens or sonic resonance tests on TRM coupons) has provided satisfactory results, when compared with destructive tests data; it can be concluded that these techniques may be very appropriate for the evaluation of damage by high temperature exposure in this type of materials.
- At room temperature, the tensile behavior of TRMs is different depending on the type of mesh used. In carbon or basalt fiber meshes, a bilinear response and a well-defined ultimate strength point is observed, as a consequence of fiber rupture. In case of glass fiber meshes, the stress-strain curves show higher dispersions and the ultimate strength point cannot be clearly identified in all cases (in these series a second branch is obtained with very little slope, where the deformations increase at approximately constant tension as a result of the fibers slippage inside the mortar matrix).
- At moderate temperature levels (up to 200 °C) the 4 materials studied keep their mechanical properties relatively unaltered. In fact, in some cases, improvements in the strength capacity of TRMs at these temperature levels have been obtained. These improvements are attributed, on the one hand, to the shrinkage of the mortar matrix during the cooling process, increasing the bond with the fibers; on the other hand, such improvements are observed in polymer-coated meshes, in which fiber-mortar adhesion is increased when the coating is softened by the effect of heat.
- At 400 °C a significant loss of strength is detected in all cases, and only TRMs with carbon fibers seem to retain some mechanical

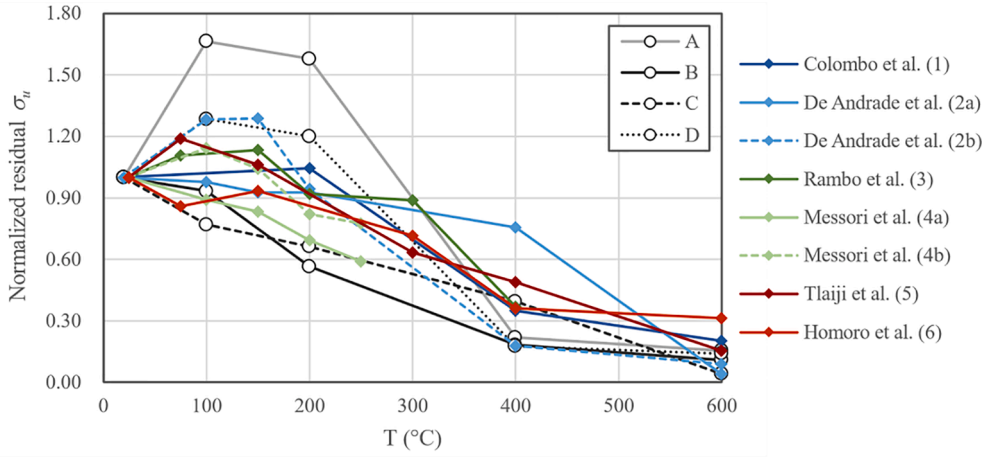

Fig. 14. Ultimate tensile stress loss with temperature exposure: comparison with other studies.

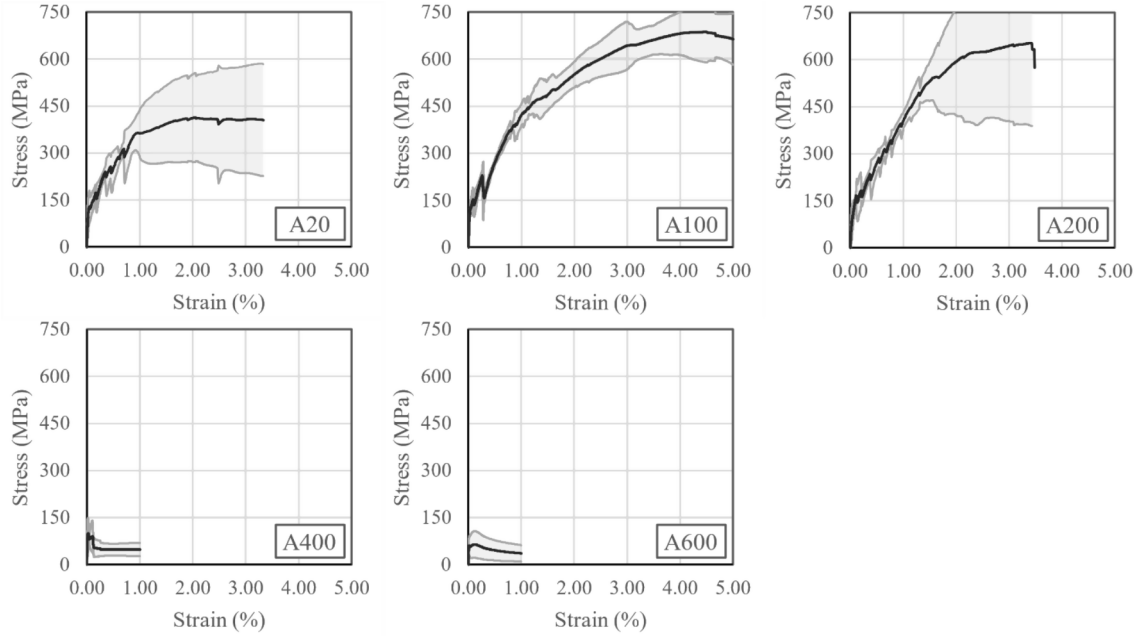

Fig. A1. Experimental stress-strain curves for A-series.

capacity (these meshes are the only ones which are not coated). At 600 °C the material is strongly damaged in all cases, the meshes appear completely degraded and the adhesion to the mortar matrix is lost. The results obtained are consistent with those reported in other published works with TRMs subjected to high temperature exposure.

- As a summary and main conclusion of this work, it is worth highlighting that TRMs are often wrongly perceived as fire resistant systems, due to the inherent non-combustibility character of inorganic mortars, compared to organic resins of FRPs. However, these materials may require additional protections in many cases, as it has been found that at 600 °C (which is the usual range of temperatures that can be reached during a fire inside a building) their mechanical properties are severely compromised.

Finally, it is important to highlight that these conclusions are limited to the commercial TRM solutions tested in this study. In this regard, some parameters of potential relevance are suggested for future research: (i) in this work, only lime-based mortars have been used, so other types of matrices could be studied, and including additions or fibers to improve the behavior at high temperature; (ii) in the coupons tested only one layer of fabric was used in all cases, so another parameter of study could be to increase the number of layers and analyze its effect; (iii) it has been shown that the type of coating polymer can significantly influence mesh-to-matrix bond at high temperature, so it could be of great interest to study specifically the behavior of a same TRM with different coatings and temperature levels.

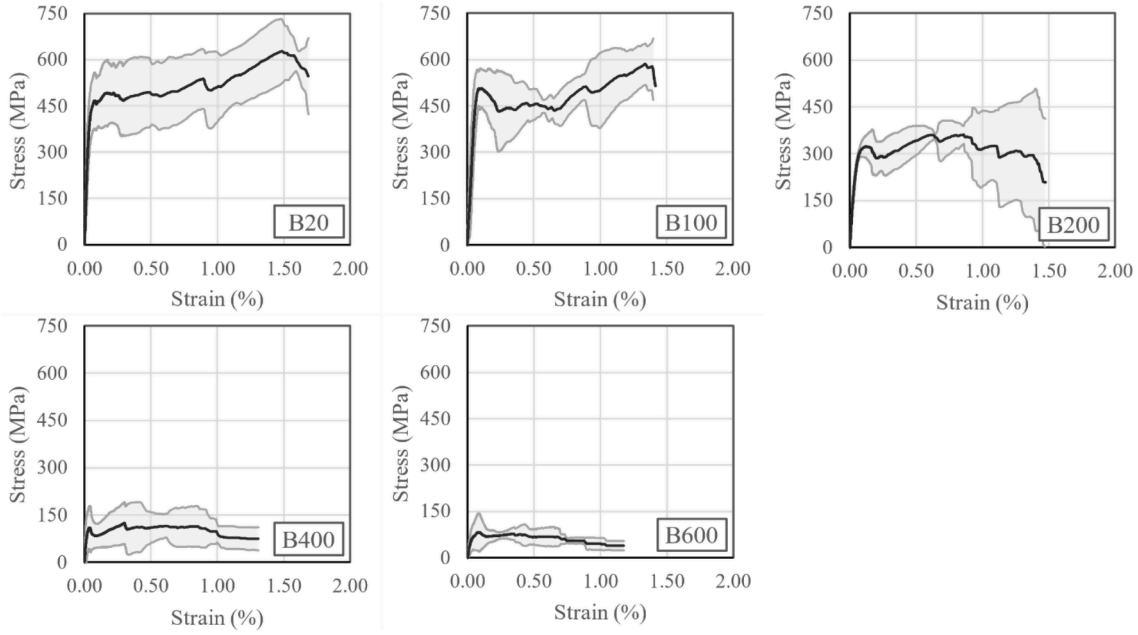

Fig. A2. Experimental stress-strain curves for B-series.

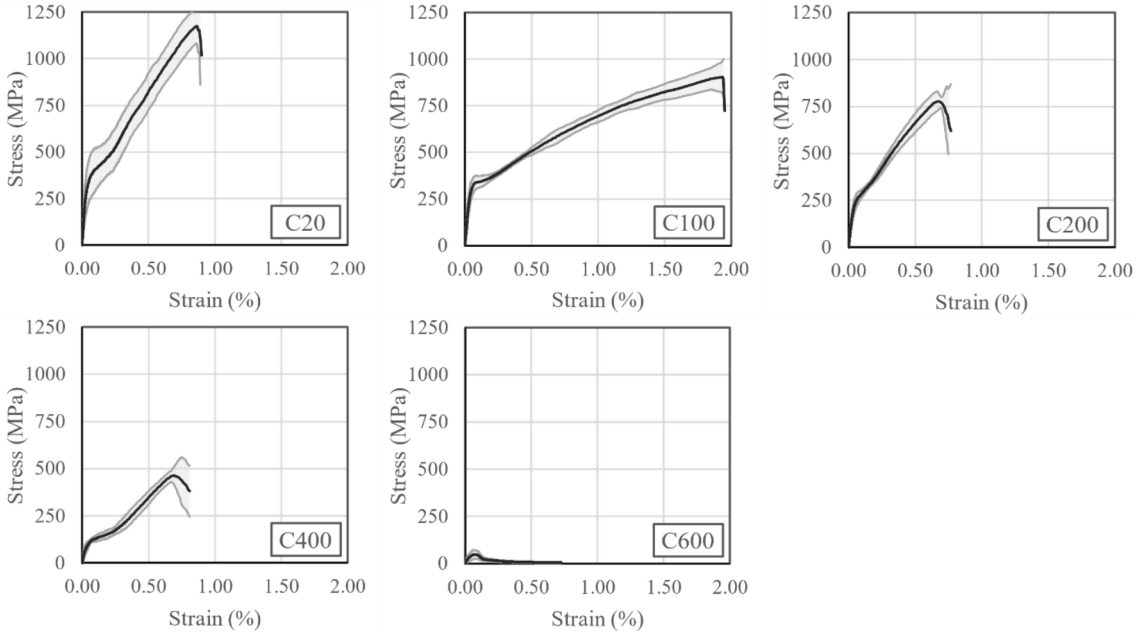

Fig. A3. Experimental stress-strain curves for C-series.

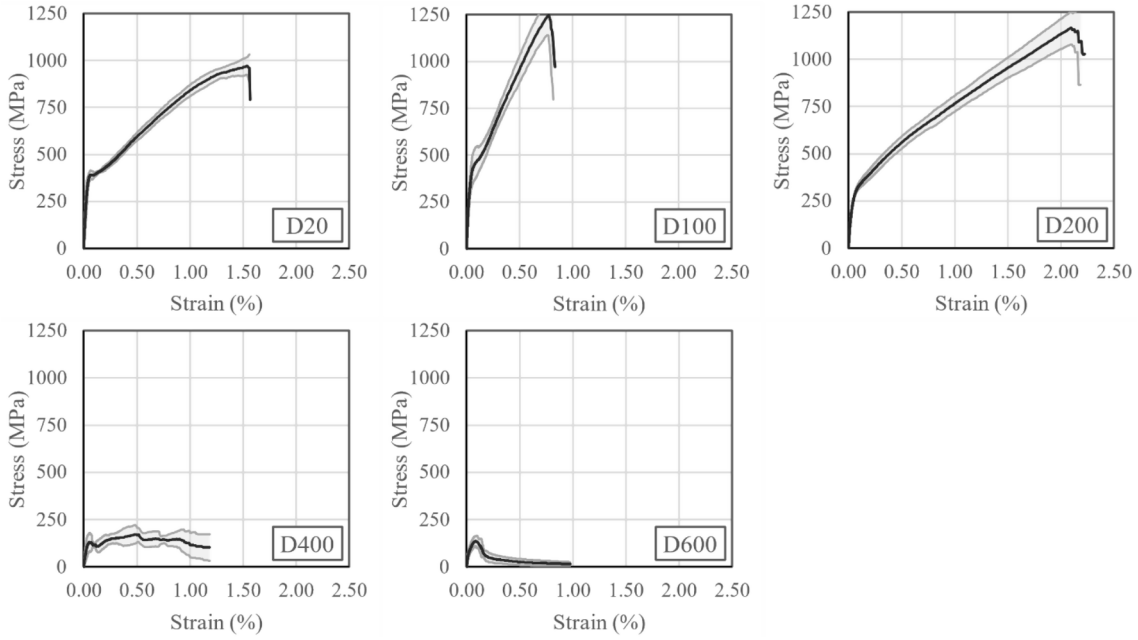

Fig. A4. Experimental stress-strain curves for D-series.

CRediT authorship contribution statement

Luis Estevan: Formal analysis, Investigation, Writing – original draft, Visualization. **Francisco B. Varona:** Investigation, Writing – review & editing, Project administration, Funding acquisition. **F. Javier Baeza:** Conceptualization, Investigation, Writing – review & editing, Supervision. **Benjamín Torres:** Methodology, Investigation, Resources, Visualization. **David Bru:** Methodology, Validation, Investigation.

Declaration of Competing Interest

The authors declare that they have no known competing financial interests or personal relationships that could have appeared to influence the work reported in this paper.

Acknowledgements

The authors would like to acknowledge Mapei Spain S.A. for the materials supplied in this work. This research has been funded by the Spanish Ministry of Science, Innovation and Universities, grant number RTI2018-101148-B-100.

Appendix A

The stress-strain curves of the 20 series tested are presented in this appendix. In each graph, the average of the 4 specimens that make up

each set is represented by a dark line. The bilateral 90% confidence intervals of the strength, determined for each strain value, are shaded in gray. In this way, the dispersions obtained in each case can be easily visualized (Figs. A1–A4).

References

[1] M.Z. Naser, R.A. Hawileh, J.A. Abdalla, Fiber-reinforced polymer composites in strengthening reinforced concrete structures: A critical review, Eng. Struct. 198 (2019) 109542, https://doi.org/10.1016/j.engstruct.2019.109542.

[2] L.A.S. Kouris, T.C. Triantafillou, State-of-the-art on strengthening of masonry structures with textile reinforced mortar (TRM), Constr. Build. Mater. 188 (2018) 1221–1233, https://doi.org/10.1016/j.conbuildmat.2018.08.039.

[3] L.N. Koutas, Z. Tetta, D.A. Bournas, T.C. Triantafillou, Strengthening of Concrete Structures with Textile Reinforced Mortars: State-of-the-Art Review, J. Compos. Constr. 23 (1) (2019) 03118001.

[4] S. Ivorra, B. Torres, F.J. Baeza, D. Bru, In-plane shear cyclic behavior of windowed masonry walls reinforced with textile reinforced mortars, Eng. Struct. 226 (2021) 111343, https://doi.org/10.1016/j.engstruct.2020.111343.

[5] B. Torres, S. Ivorra, F. Javier Baeza, L. Estevan, B. Varona, Textile reinforced mortars (TRM) for repairing and retrofitting masonry walls subjected to in-plane cyclic loads. An experimental approach, Eng. Struct. 231 (2021) 111742, https://doi.org/10.1016/j.engstruct.2020.111742.

[6] L. Estevan, F.J. Baeza, D. Bru, S. Ivorra, Stone masonry confinement with FRP and FRCM composites, Constr. Build. Mater. 237 (2020) 117612, https://doi.org/10.1016/j.conbuildmat.2019.117612.

[7] A. Cascardi, F. Micelli, M.A. Aiello, FRCM-confined masonry columns: experimental investigation on the effect of the inorganic matrix properties, Constr. Build. Mater. 186 (2018) 811–825, https://doi.org/10.1016/j.conbuildmat.2018.08.020.

[8] F.A. Kariou, S.P. Triantafyllou, D.A. Bournas, TRM strengthening of masonry arches: An experimental investigation on the effect of strengthening layout and textile fibre material, Compos. Part B Eng. 173 (2019) 106765.

[9] E. Bertolesi, B. Torres, J.M. Adam, P.A. Calderón, J.J. Moragues, Effectiveness of Textile Reinforced Mortar (TRM) materials for the repair of full-scale timbrel masonry cross vaults, Eng. Struct. 220 (2020) 110978, https://doi.org/10.1016/j.engstruct.2020.110978.

[10] H.M. Elsanadedy, T.H. Almusallam, S.H. Alsayed, Y.A. Al-Salloum, Flexural strengthening of RC beams using textile reinforced mortar - Experimental and numerical study, Compos. Struct. 97 (2013) 40–55, https://doi.org/10.1016/j.compstruct.2012.09.053.

[11] L.N. Koutas, D.A. Bournas, Flexural Strengthening of Two-Way RC Slabs with Textile-Reinforced Mortar: Experimental Investigation and Design Equations, J. Compos. Constr. 21 (1) (2017) 04016065, https://doi.org/10.1061/(ASCE)CC.1943-5614.0000713.

[12] Z.C. Tetta, L.N. Koutas, D.A. Bournas, Textile-reinforced mortar (TRM) versus fiber-reinforced polymers (FRP) in shear strengthening of concrete beams, Compos. Part B Eng. 77 (2015) 338–348, https://doi.org/10.1016/j.compositesb.2015.03.055.

[13] P. Colajanni, F. De Domenico, A. Recupero, N. Spinella, Concrete columns confined with fibre reinforced cementitious mortars: Experimentation and modelling, Constr. Build. Mater. 52 (2014) 375–384, https://doi.org/10.1016/j.conbuildmat.2013.11.048.

[14] F. Faleschini, M.A. Zanini, L. Hofer, C. Pellegrino, Experimental behavior of reinforced concrete columns confined with carbon-FRCM composites, Constr. Build. Mater. 243 (2020) 118296, https://doi.org/10.1016/j.conbuildmat.2020.118296.

[15] ACI 549.4R-20, Guide to Design and Construction of Externally Bonded Fabric-Reinforced Cementitious Matrix and Steel-Reinforced Grout Systems for Repair and Strengthening of Concrete Structures, American Concrete Institute, ACI Committee 549, (2020).

[16] CNR-DT 215/2018, Guide for the Design and Construction of Externally Bonded Fibre Reinforced Inorganic Matrix Systems for Strengthening Existing Structures, CNR - Advisory Committee on Technical Recommendations for Construction, Rome, Italy, (2020).

[17] J. Donnini, V. Corinaldesi, A. Nanni, Mechanical properties of FRCM using carbon fabrics with different coating treatments, Compos. Part B Eng. 88 (2016) 220–228, https://doi.org/10.1016/j.compositesb.2015.11.012.

[18] O. Homoro, M. Michel, T.N. Baranger, Dry mineral pre-impregnation for enhancing the properties of glass FRCM composites, Constr. Build. Mater. 263 (2020) 120597, https://doi.org/10.1016/j.conbuildmat.2020.120597.

[19] AC434, Acceptance Criteria for Masonry and Concrete Strengthening Using Fiber-Reinforced Cementitious Matrix (FRCM) Composite Systems, ICC Evaluation Service, (2016).

[20] RILEM Technical Committee 232-TDT (Wolfgang Brameshuber), Recommendation of RILEM TC 232-TDT: test methods and design of textile reinforced concrete. Uniaxial tensile test: test method to determine the load bearing behavior of tensile specimens made of textile reinforced concrete, Mater. Struct. 49 (2016) 4923–4927. https://doi.org/10.1617/s11527-016-0839-z.

[21] F.G. Carozzi, A. Bellini, T. D'Antino, G. de Felice, F. Focacci, Ł. Hojdys, L. Laghi, E. Lanoye, F. Micelli, M. Panizza, C. Poggi, Experimental investigation of tensile and bond properties of Carbon-FRCM composites for strengthening masonry elements, Compos. Part B Eng. 128 (2017) 100–119, https://doi.org/10.1016/j.compositesb.2017.06.018.

[22] M. Leone, M.A. Aiello, A. Balsamo, F.G. Carozzi, F. Ceroni, M. Corradi, M. Gams, E. Garbin, N. Gattesco, P. Krajewski, C. Mazzotti, D. Oliveira, C. Papanicolaou, G. Ranocchiai, F. Roscini, D. Saenger, Glass fabric reinforced cementitious matrix: Tensile properties and bond performance on masonry substrate, Compos. Part B Eng. 127 (2017) 196–214, https://doi.org/10.1016/j.compositesb.2017.06.028.

[23] G.P. Lignola, C. Caggegi, F. Ceroni, S. De Santis, P. Krajewski, P.B. Lourenço, M. Morganti, C. Papanicolaou, C. Pellegrino, A. Prota, L. Zuccarino, Performance assessment of basalt FRCM for retrofit applications on masonry, Compos. Part B Eng. 128 (2017) 1–18.

[24] C. Caggegi, E. Lanoye, K. Djama, A. Bassil, A. Gabor, Tensile behaviour of a basalt TRM strengthening system: Influence of mortar and reinforcing textile ratios, Compos. Part B Eng. 130 (2017) 90–102, https://doi.org/10.1016/j.compositesb.2017.07.027.

[25] T. D'Antino, C. Papanicolaou, Mechanical characterization of textile reinforced inorganic-matrix composites, Compos. Part B Eng. 127 (2017) 78–91, https://doi.org/10.1016/j.compositesb.2017.02.034.

[26] B. Li, H. Xiong, J. Jiang, X. Dou, Tensile behavior of basalt textile grid reinforced Engineering Cementitious Composite, Compos. Part B Eng. 156 (2019) 185–200, https://doi.org/10.1016/j.compositesb.2018.08.059.

[27] Ł. Hojdys, P. Krajewski, Tensile behaviour of frcm composites for strengthening of masonry structures—an experimental investigation, Materials (Basel). 14 (13) (2021) 3626, https://doi.org/10.3390/ma14133626.

[28] A. Bilotta, F. Ceroni, G.P. Lignola, A. Prota, Use of DIC technique for investigating the behaviour of FRCM materials for strengthening masonry elements, Compos. Part B Eng. 129 (2017) 251–270, https://doi.org/10.1016/j.compositesb.2017.05.075.

[29] B. Torres, F.B. Varona, F.J. Baeza, D. Bru, S. Ivorra, Study on retrofitted masonry elements under shear using digital image correlation, Sensors (Switzerland). 20 (7) (2020) 2122, https://doi.org/10.3390/s20072122.

[30] S. De Santis, F.G. Carozzi, G. de Felice, C. Poggi, Test methods for Textile Reinforced Mortar systems, Compos. Part B Eng. 127 (2017) 121–132, https://doi.org/10.1016/j.compositesb.2017.03.016.

[31] S. De Santis, H.A. Hadad, F. De Caso y Basalo, G. de Felice, A. Nanni, Acceptance Criteria for Tensile Characterization of Fabric-Reinforced Cementitious Matrix Systems for Concrete and Masonry Repair, J. Compos. Constr. 22 (6) (2018) 04018048.

[32] L. Bisby, Fire Resistance of Textile Fiber Composites Used in Civil Engineering, in: Text. Fibre Compos. Civ. Eng., 2016: pp. 169–185. https://doi.org/10.1016/B978-1-78242-446-8.00008-2.

[33] C.C. Papanicolaou, T. Triantafillou, Performance of TRM/TRC systems under elevated temperatures and fire conditions, in: Am. Concr. Institute, ACI Spec. Publ., 2021: pp. 32–46.

[34] I. Colombo, M. Colombo, A. Magri, G. Zani, M. Di Prisco, Textile reinforced mortar at high temperatures, Appl. Mech. Mater. 82 (2011) 202–207, https://doi.org/10.4028/www.scientific.net/AMM.82.202.

[35] F.D.A. Silva, M. Butler, S. Hempel, R.D. Toledo Filho, V. Mechtcherine, Effects of elevated temperatures on the interface properties of carbon textile-reinforced concrete, Cem. Concr. Compos. 48 (2014) 26–34, https://doi.org/10.1016/j.cemconcomp.2014.01.007.

[36] D.A.S. Rambo, F. de Andrade Silva, R.D. Toledo Filho, O. da Fonseca Martins Gomes, Effect of elevated temperatures on the mechanical behavior of basalt textile reinforced refractory concrete, Mater. Des. 65 (2015) 24–33. https://doi.org/10.1016/j.matdes.2014.08.060.

[37] D.A.S. Rambo, Y. Yao, F. de Andrade Silva, R.D. Toledo Filho, B. Mobasher, Experimental investigation and modelling of the temperature effects on the tensile behavior of textile reinforced refractory concretes, Cem. Concr. Compos. 75 (2017) 51–61, https://doi.org/10.1016/j.cemconcomp.2016.11.003.

[38] J. Donnini, F. De Caso y Basalo, V. Corinaldesi, G. Lancioni, A. Nanni, Fabric-reinforced cementitious matrix behavior at high-temperature: Experimental and numerical results, Compos. Part B Eng. 108 (2017) 108–121.

[39] M. Messori, A. Nobili, C. Signorini, A. Sola, Effect of high temperature exposure on epoxy-coated glass textile reinforced mortar (GTRM) composites, Constr. Build. Mater. 212 (2019) 765–774, https://doi.org/10.1016/j.conbuildmat.2019.04.026.

[40] T.H. Nguyen, X.H. Vu, A. Si Larbi, E. Ferrier, Experimental study of the effect of simultaneous mechanical and high-temperature loadings on the behaviour of textile-reinforced concrete (TRC), Constr. Build. Mater. 125 (2016) 253–270, https://doi.org/10.1016/j.conbuildmat.2016.08.026.

[41] T. Tlaiji, X.H. Vu, E. Ferrier, A. Si Larbi, Thermomechanical behaviour and residual properties of textile reinforced concrete (TRC) subjected to elevated and high temperature loading: Experimental and comparative study, Compos. Part B Eng. 144 (2018) 99–110, https://doi.org/10.1016/j.compositesb.2018.02.022.

[42] O. Homoro, X.H. Vu, E. Ferrier, Experimental and analytical study of the thermo-mechanical behaviour of textile-reinforced concrete (TRC) at elevated temperatures: Role of discontinuous short glass fibres, Constr. Build. Mater. 190 (2018) 645–663, https://doi.org/10.1016/j.conbuildmat.2018.09.142.

[43] N.H. Dinh, S.-H. Park, K.-K. Choi, Effect of dispersed micro-fibers on tensile behavior of uncoated carbon textile-reinforced cementitious mortar after high-temperature exposure, Cem. Concr. Compos. 118 (2021) 103949, https://doi.org/10.1016/j.cemconcomp.2021.103949.

[44] ASTM D2845-08, Standard Test Method for Laboratory Determination of Pulse Velocities and Ultrasonic Elastic Constants of Rock, ASTM International, West Conshohocken, PA, (2008).
[45] ASTM E1875-20a, Standard Test Method for Dynamic Young's Modulus, Shear Modulus, and Poisson's Ratio by Sonic Resonance, ASTM International, West Conshohocken, PA, (2020).
[46] UNE-EN 1015-11:2020, Methods of test for mortar for masonry - Part 11: Determination of flexural and compressive strength of hardened mortar, (2020).